Electronic Supplementary Material (ESI) for Journal of Materials Chemistry C.

Supplementary Information

Schottky Photodiodes Based on Mid-Wavelength Infrared Intraband Colloidal Quantum Dots – Surface Ligand and Metal Contact Studies

Mohammad M. Al Mahfuz[a], Junsung Park[a], Rock Huebner[b], Sunghwan Lee[c], Dong-Kyun Ko[a,]*

[a] Department of Electrical and Computer Engineering, New Jersey Institute of Technology, Newark, NJ 07102, United States

[b] Department of Mechanical and Industrial Engineering, New Jersey Institute of Technology, Newark, NJ 07102, United States

[c] School of Engineering Technology, Purdue University, West Lafayette, IN 47907, United States

* Corresponding author. E-mail address: dkko@njit.edu

S1. Optimization of binary CQD mixture ratio

First using Ag_2Se and PbS CQDs, solutions were prepared with identical concentrations of 40 mg/mL. Binary CQD mixture solutions were prepared with different volume ratios, where 5/750 corresponds to 5 μL of Ag_2Se CQD and 750 μL PbS CQD mixture solution. To systematically investigate the wide range of mixture compositions, we have prepared 5 different solution mixtures by increasing the Ag_2Se CQD loading by 10 times (5/750, 50/750, 500/750, 500/75, and 500/7.5). Upward-looking, vertically-stacked devices were fabricated using Au as top and bottom electrodes (as shown in Fig. S1 (a)) and 1,2-ethanedithiol as ligands. The key parameters that determine the performance of a photodetector are the infrared responsivity (R) and dark current (I_{dark}). These two parameters are used as a main criterion to determine binary mixture optimization.

Fig. S1 below shows the device measurement results. First, we observe that with increasing Ag_2Se CQD loading, infrared responsivity increases to a peak at 50/750 mixture with some devices exhibiting responsivities as high as 0.7 A/W at room temperature. We also observe that the devices with Ag_2Se CQD loading in the excess of 500/750 show very low device resistivities, such that photocurrent could not be measured using lock-in techniques (sample impedance out of range, denoted as X-marked box in Fig. S1(b). In fact, this is expected due to the degenerately-doped nature of intraband Ag_2Se CQDs. Unlike traditional CQDs where electrons occupy up to the maximum valence energy levels, Ag_2Se CQDs have electrons filled up to the first quantum confined conduction level (heavily electron-doped), hence giving rise to intraband transitions. In our CQD mixture film – note that 5.5 nm Ag_2Se CQDs are almost the twice the size of 3 nm PbS CQDs – increasing the Ag_2Se CQDs loading increases the probability of creating direct percolation paths across the top and bottom electrode, resulting in low electrical resistance. This is depicted in Fig. S1(c) - in our CQD mixture devices, this occurs above 500/750 Ag_2Se CQD loading. The

device resistivity is measured as a function of Ag_2Se CQD loading, as shown in Fig. S1(d). The resistivity values show a sudden decrease near 500/750, collaborating this hypothesis.

From this work, we conclude that the optimum Ag_2Se CQD loading lies approximately at 50 /750. The infrared optical absorption taken from 50/750 mixture film is also shown in Fig. S1(e).

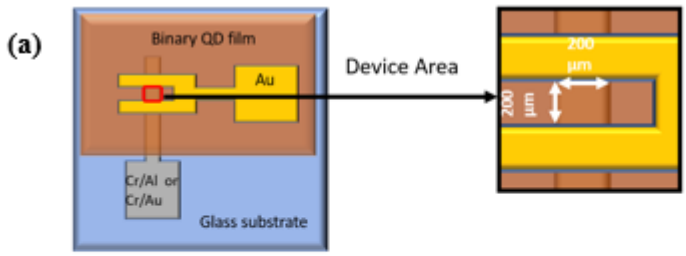

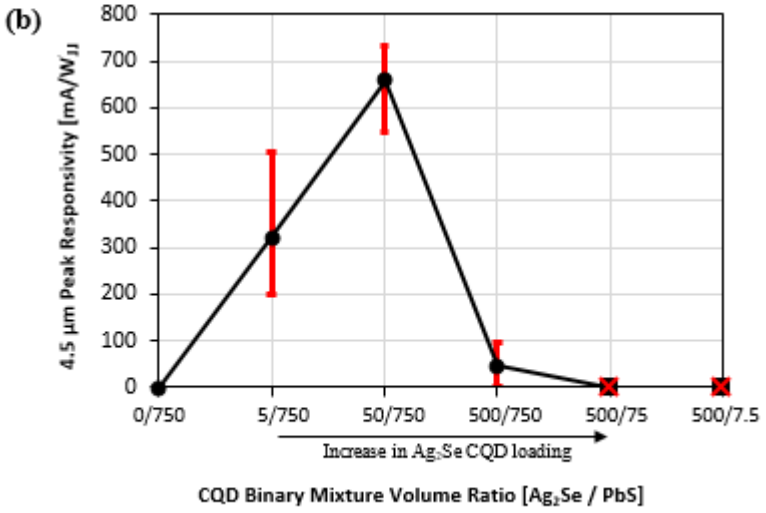

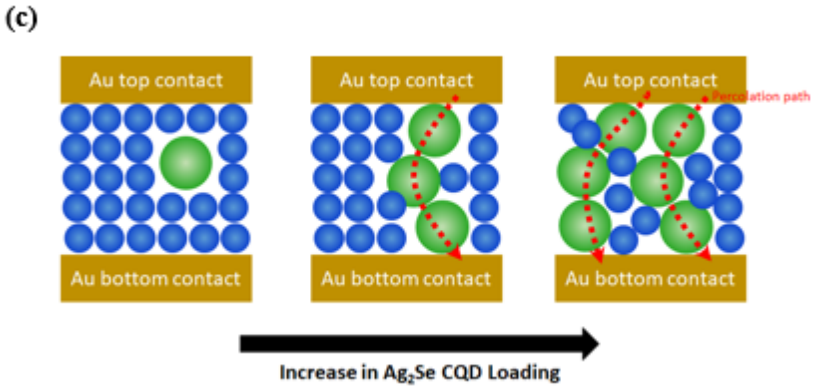

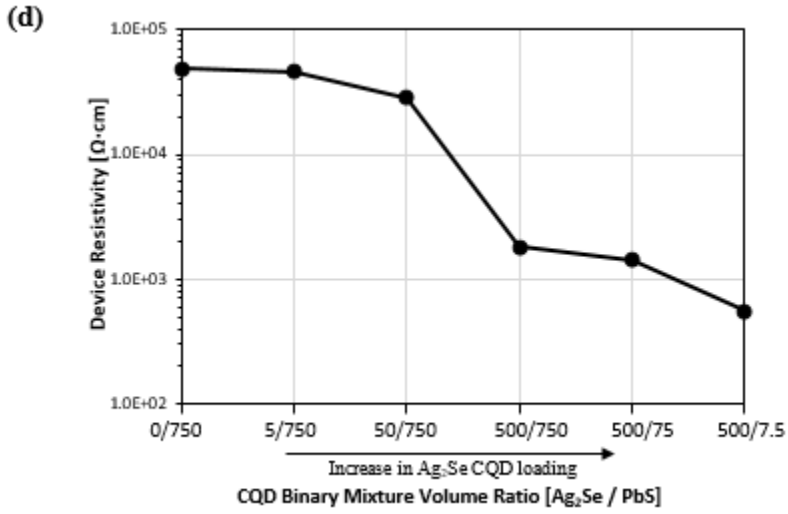

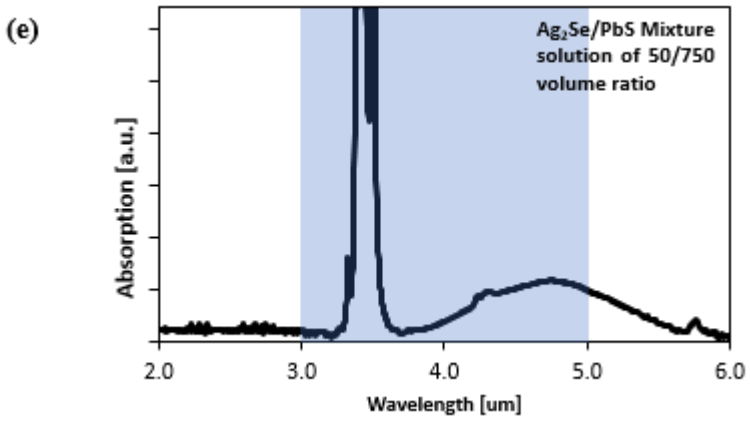

Fig. S1 (a) Upward-looking, vertical device structure (b) Plot of 4.5 μm peak responsivities, (c) schematic depicting the creation of percolation path, and (d) plot of device resistivities as a function of increasing Ag_2Se CQD loading. (e) shows infrared optical absorption of a film with CQDs mixture solution of 50/750 volume ratio.

S2. Summary of ligands studied in this work

Table below summarizes the five ligands that was studied in this work.

Type of Ligands	**Dark Resistivity (Ohm.cm)**	**MWIR Responsivity at 4.5 µm, 0.9V Bias (mA/W)**	**Contact Property with Au**	**Sensitivity Ratio (I_{photo}/I_{dark})**	**Ligand Exchange Procedure**
1,2-Ethandithiol (EDT)	**$2.3x10^4$** (slope of linear plot)	**732.53**	**Ohmic**	**$2.4X10^{-4}$**	**Solvent:** Acetonitrile **Concentration:** 10mM **Dipping time:** 20Sec
1,3-Benzenedithiol (BDT)	**$6.4x10^7$** (slope of linear plot)	**1.41**	**Ohmic**	**$2.9X10^{-3}$**	**Solvent:** Acetonitrile **Concentration:** 1.7mM **Dipping time:** 20Sec
3-Mercaptopropionic acid (MPA)	**$8.3x10^5$** (slope of linear plot)	**37.63**	**Ohmic**	**$1.6X10^{-3}$**	**Solvent:** Acetonitrile **Concentration:** 50mM **Dipping time: 20Sec**
Ammonium thiocyanate (SCN)	**$6.2\ x10^4$** (from reverse-biased region)	**120.97**	**Schottky**	**$1.4X10^{-4}$**	**Solvent:** Acetonitrile **Concentration:** 100mM **Dipping time:** 20Sec
Tetrabutylammonium iodide (TBAI)	**$2.2\ x10^6$** (from reverse-biased region)	**No responsivity at 0.9V**	**Schottky**	**-**	**Solvent:** Acetonitrile **Concentration:** 10mg/ml **Dipping time:** 20Sec

S3. Transmission Spectra of Binary CQD Different Ligands

Fig. S2 shows transmission spectra of different ligand-treated CQD films obtained through combined near IR and FTIR measurements. The ligand exchange of films containing intraband CQDs are known to induce mid-infrared optical absorbance/transmittance change due to carrier doping or de-doping effect[1] and we also observe the same effects in this study (see TBAI), as shown in the figure below.

Previous CQD study[2] has reported that ligands can shift the entire energy level of the CQD with respect to the reference vacuum level. In connection to the environmental Fermi level doping mechanism in intraband CQDs,[3-5] the electron population of $1S_e$ in Ag_2Se CQD, hence the MWIR absorption strength, should increase in the order MPA < EDT < BDT < SCN < TBAI (until $1S_e$ is fully filled and $1P_e$ starts to become populated). However, we observe minimal changes in the MWIR absorbance, especially across MPA, EDT, BDT, and SCN ligands, indicating that more complex doping mechanisms are at play.

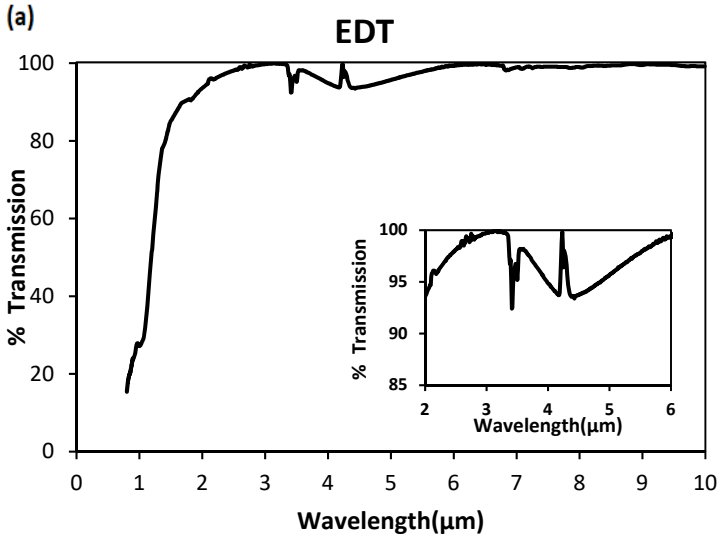

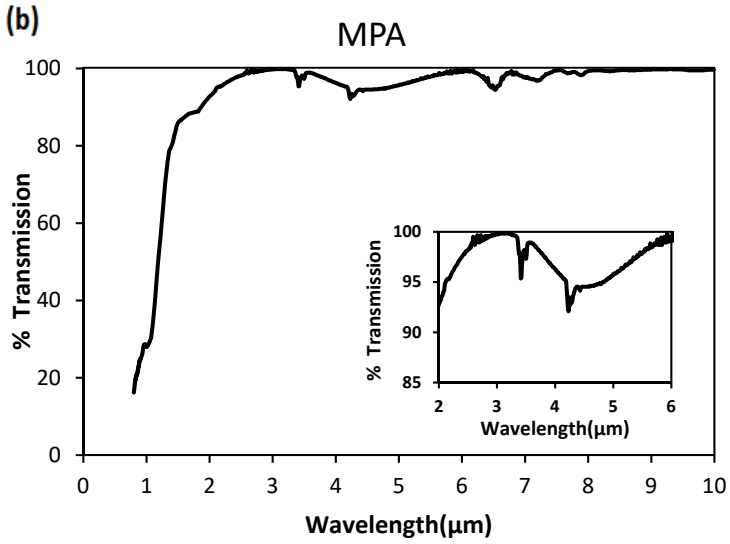
(b)
MPA
% Transmission
Wavelength(µm)
100
80
60
40
20
0
0 1 2 3 4 5 6 7 8 9 10
100
95
90
85
2 3 4 5 6

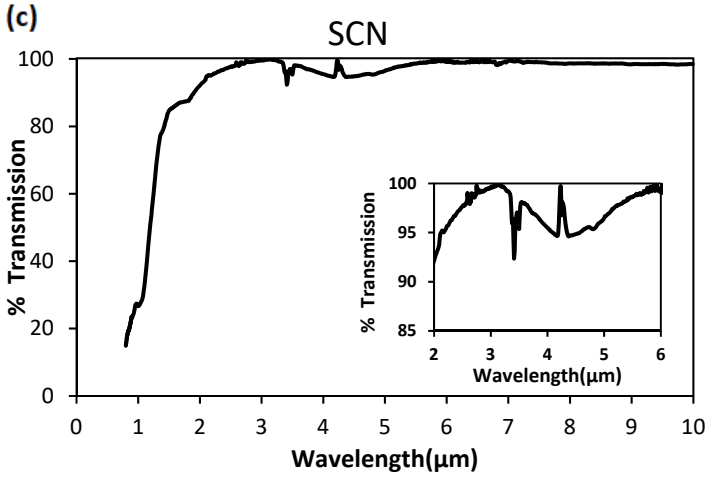
(c)
SCN
% Transmission
Wavelength(µm)
100
80
60
40
20
0
0 1 2 3 4 5 6 7 8 9 10
100
95
90
85
2 3 4 5 6

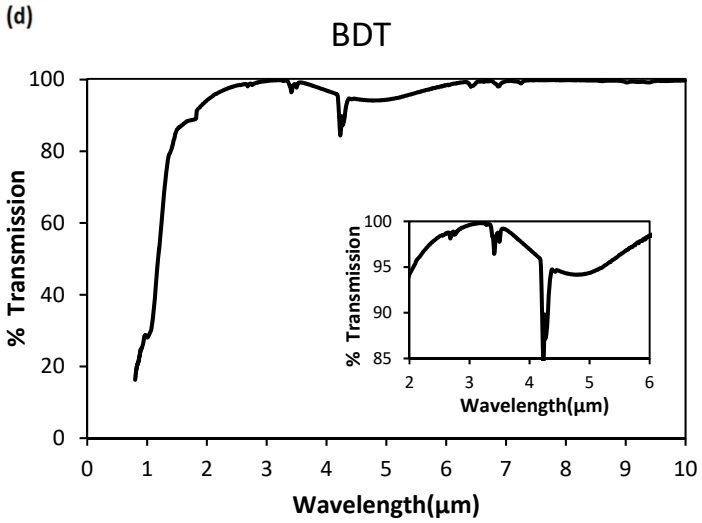
(d)
BDT
% Transmission
Wavelength(µm)
100
80
60
40
20
0
0 1 2 3 4 5 6 7 8 9 10
100
95
90
85
2 3 4 5 6

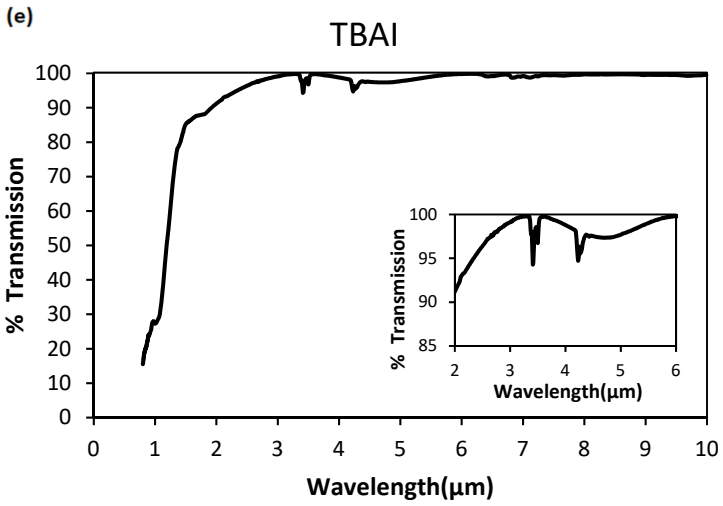

Fig. S2 Optical transmittance of films obtained from binary mixture (500µl/750µl Ag2Se/PbS) CQDs, treated with (a) EDT,(b) MPA,(c) SCN,(d) BDT and (e) TBAI ligands. Magnified view of MWIR regions are included as insets.

S4. I-V characteristics of organic vs inorganic ligand

Fig. S3 below shows the I-V characteristics, plotted in linear scale, of representative organic (EDT) and inorganic (TBAI) ligands, showing a clear quasi-linear and rectifying characteristic, respectively.

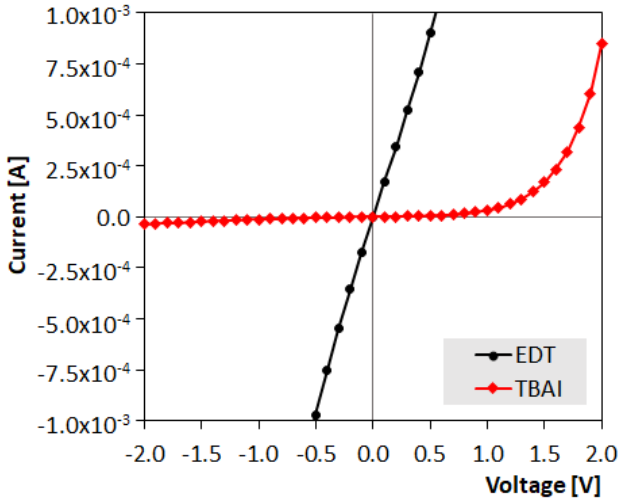

Fig. S3 Current-voltage (I-V) characteristics of EDT and TBAI ligands plotted in linear current scale.

S5. Temporal photocurrent of Schottky devices

Fig. S4 below shows the photocurrent vs. time plot of an EDT-ligand exchanged binary CQD Schottky device, under 0.75V bias. Under light (3-5 μm MWIR illumination), a distinct photocurrent of ~ 1 μA arises.

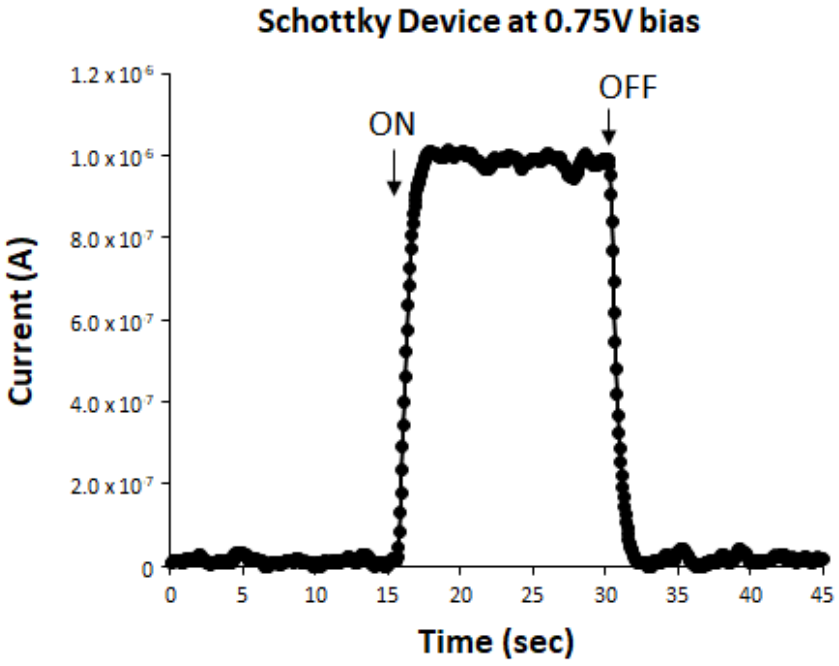

Fig. S4 Photocurrent vs. time plot obtained from EDT-ligand exchanged binary CQD Schottky device.

S6. TEM size distribution analysis and optical absorption broadening

Fig. S5 shows the TEM size distribution analysis. The full width at half maximum (FWHM) of the energy broadening was calculated following the reference,[6,7] using the equation:

$$E = \frac{-E_G}{2} + \sqrt{\left(\frac{E_G}{2}\right)^2 + \mathrm{A^2k^2}}$$

Ak is the matrix element of the perturbing potential. For Ag_2Se quantum dot with radius R, the K values are π /R and 4.49/R for $1S_e$ and $1P_e$ level respectively. The calculated FWHM energy broadening of 126 meV is in close agreement with the broadening estimated from the optical absorption of the MWIR peak (FWHM of 97 meV) shown in Fig. 2c in the main text.

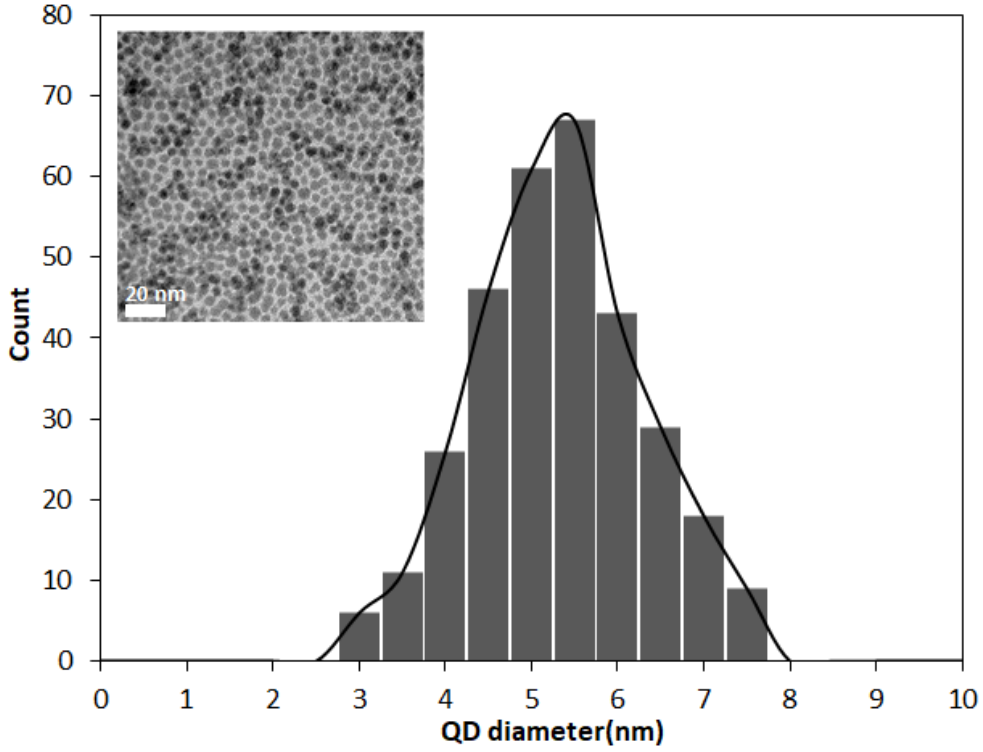

Fig. S5 Histogram showing Ag_2Se CQD diameter calculated from TEM image (inset).

A publication by J. Son et al.[7] describes the splitting of $1P_e$ level in Ag_2Se CQDs. This level splitting will broaden the measured $1S_e$-$1P_e$ absorption peak. However, the splitting only occurs for larger CQD sizes (intraband absorption peak above 6 µm, see Figure S6). The Ag_2Se CQDs used in this device study are small (red curve below, intraband peak at 4.5 um) and the splitting of $1P_e$ level is yet to occur. Hence, we conclude that the absorption broadening of our data is mainly attributed to the size dispersion in CQD samples.

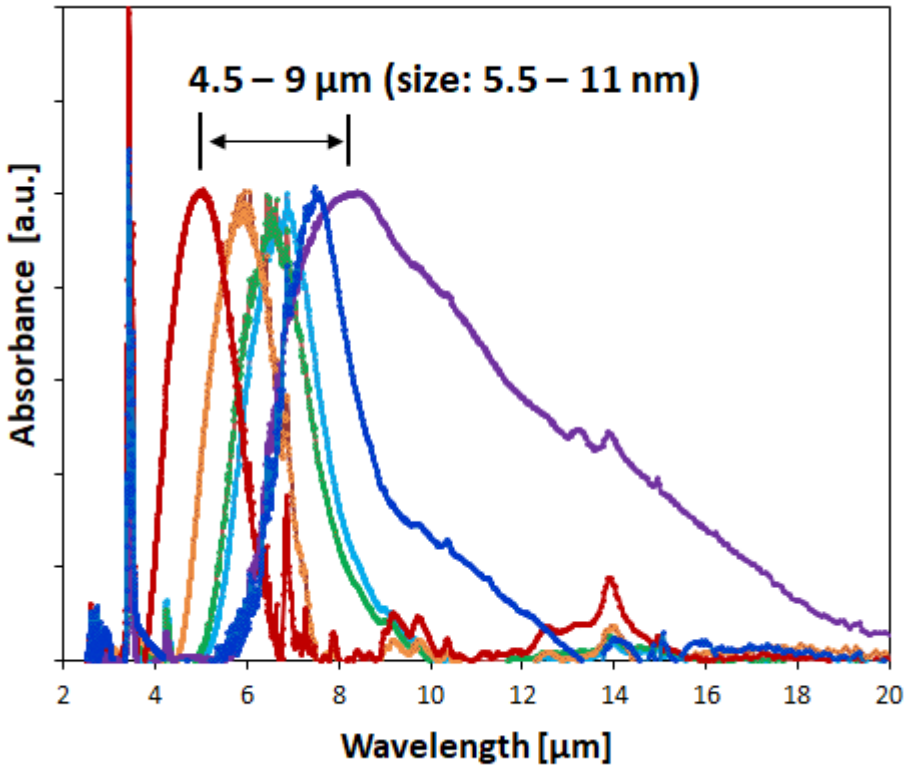

Fig. S6 Optical Absorption Spectra of Ag_2Se of different sizes

References:

1 A. Robin, C. Livache, S. Ithurria, E. Lacaze, B. Dubertret and E. Lhuillier, ACS Appl. Mater. Interfaces, 2016, 8, 27122–27128.

2 P. R. Brown, D. Kim, R. R. Lunt, N. Zhao, M. G. Bawendi, J. C. Grossman and V. Bulović, ACS Nano, 2014, 8, 5863–5872.

3 M. R. Scimeca, N. Mattu, I. J. Paredes, M. N. Tran, S. J. Paul, E. S. Aydil and A. Sahu, The Journal of Physical Chemistry C, 2021, 125, 17556–17564.

4 M. Chen and P. Guyot-Sionnest, ACS Nano, 2017, 11, 4165–4173.

5 G. Shen and P. Guyot-Sionnest, J. Phys. Chem. C, 2016, 120, 11744–11753.

6 M. Park, D. Choi, Y. Choi, H. Shin and K. S. Jeong, *ACS Photonics,* 2018, 5, 1907–1911.

7 J. Son, D. Choi, M. Park, J. Kim and K. S. Jeong, *Nano Lett.,* 2020, 20, 4985–4992.